J Comput Neurosci (2012) 32:25–53
DOI 10.1007/s10827-011-0335-y

Hallucinogen persisting perception disorder in neuronal networks with adaptation

Zachary P. Kilpatrick · G. Bard Ermentrout

Received: 19 January 2011 / Revised: 11 April 2011 / Accepted: 19 April 2011 / Published online: 14 June 2011

Abstract We study the spatiotemporal dynamics of neuronal networks with spike frequency adaptation. In particular, we compare the effects of adaptation being either a linear or nonlinear function of neural activity. We find that altering parameters controlling the strength of synaptic connections in the network can lead to spatially structured activity suggestive of symptoms of hallucinogen persisting perception disorder (HPPD). First, we study how both networks track spatially homogeneous flickering stimuli, and find input is encoded as continuous at lower flicker frequencies when the network's synapses exhibit more net excitation. Mainly, we study instabilities of stimulus-driven traveling pulse solutions, representative of visual trailing phenomena common to HPPD patients. Visual trails are reported as discrete afterimages in the wake of a moving input. Thus, we analyze several solutions arising in response to moving inputs in both networks: an ON state, stimulus-locked pulses, and traveling breathers. We find traveling breathers can arise in both networks when an input moves beyond a critical speed. These possible neural substrates of visual trails occur at slower speeds when the modulation of synaptic connectivity is increased.

Keywords Hallucinations · Neuronal networks · Spike frequency adaptation · Traveling waves · Breathers

Action Editor: P. Dayan

Z. P. Kilpatrick ( ) · G. Bard Ermentrout
Department of Mathematics, University of Pittsburgh,
Pittsburgh, PA 15260, USA
e-mail: zpkilpat@pitt.edu

1 Introduction

Hallucinogen persisting perception disorder (HPPD) is a malfunction wherein past users of lysergic acid diethylamide (LSD) continue to see images reminiscent of drug induced hallucinations (Halpern and Pope 2003). Similar conditions have been described as the result

in one's thoughts); and (iii) *recurrent unbidden images* (subjects see objects that are not there) (Horowitz 1969).

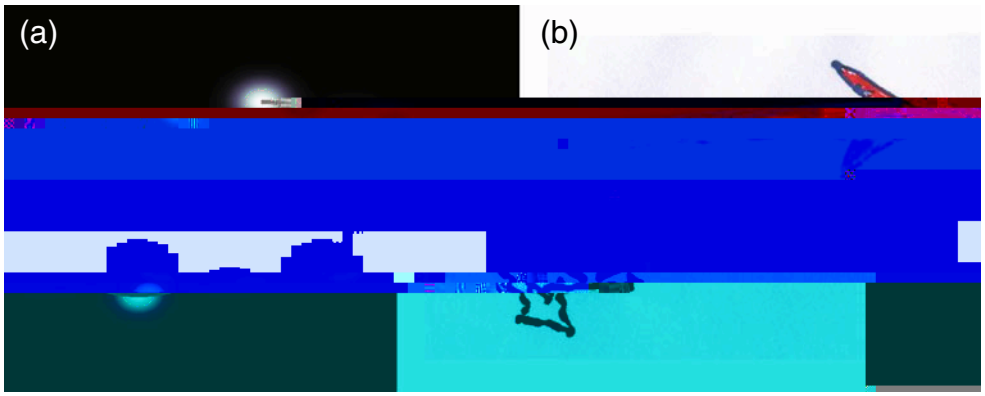

Fig. 1 (**a**) Snapshots of a spot of light rotating continuously on a circle. During visual trailing phenomena, one would see this not simply as a smoothly rotating light, but most likely discrete afterimages in addition to the smoothly rotating light image. They may also see a smudging out of the image, much like the tail of a comet. Halo phenomena lead to the observer seeing the light spot as larger than it actually is. (**b**) Drawing of a single snapshot of visual experience by an HPPD patient watching an arrow rotating counterclockwise. The *blue* and *red arrow* is the representation of the arrow's actual location, and the *faint dark arrows* are the afterimages of the arrow left in its wake. Redrawn from H. D. Abraham (2011, personal communication)

network accurately resolving the stimulus, only neurons containing the light spot in their receptive field would represent it in visual cortex at any given point in time. Due to alterations in the neurotransmitter levels of visual cortex due to LSD usage, we presume neurons will represent the stimulus in regions addition to the area of presentation in an HPPD patient. Trails are represented by spatially discrete patches of neurons in the wake of the stimulus that fire for a period of time after input has been removed. A patient's own rendering of the discrete afterimages characteristic of visual trails are pictured in Fig. 1(b), when the stimulus is an arrow rotating counterclockwise (H. D. Abraham, 2011, personal communication). Halos may also appear around the object represented by neurons around the input being continuously on. All are potential realizations of HPPD in this simple stimulus paradigm.

Large-scale spatially structured activity such as the rotating spot of activity suggested by the above experimental setup is often modeled as a standing or traveling pulse of activity in neural field models of cortex (Wilson and Cowan 1972; Amari 1977). In these models, the evolution of mean firing rate in continuous space and time can be represented by a system of dynamical equations (Coombes 2005). These often appear as integrodifferential equations that incorporate specifics of the neural system in question with a particular synaptic connectivity (or weight) function, form of firing rate function, spatial domain, and auxiliary variables representing modifications to the mean population activity. Such systems can be analyzed extensively to determine how model functions and parameters relate to the existence of different solutions like traveling waves (Pinto and Ermentrout 2001; Coombes and Owen 2004; Folias and Bressloff 2005b

current, Benda and Herz derived a neural field model where the relationship between neural activity and

waves, especially in networks with no lateral inhibition (Hansel and Sompolinsky 1998; Pinto and Ermentrout 2001; Folias and Bressloff 2005b; Troy and Shusterman 2007; Kilpatrick et al. 2008).

to the stimulus are close enough to communicate. In this case, neurons that are close to one another will excite one another and distal neurons will inhibit one another, with lateral inhibition connectivity. Analysis of the networks (2.1) and (2.2) is straightforward in the case of the harmonic weight function (2.6). However, it is conceivable that the rotating spot stimulus applied to a subject may have a circular path that is wide enough that connection strengths between some patches of neurons are effectively zero. In this case, the size of the domain would increase and we take the weight function

$$w(x-x') = e^{-|x-x'|/\sigma_e} - A_i e^{-|x-x'|/\sigma_i} \qquad |x-x'| \in [0, L] \tag{2.7}$$

where A_i parametrizes the amount of synaptic inhibition, σ_e (σ_i) the spatial scale of excitatory (inhibitory) connections, and L the spatial size of the network. The analysis of Sections 3 and 4 could be extended to a system with the weight function (2.7). Resulting formulae would merely be more tedious to derive and not as straightforward to examine. Thus, we simply perform numerical simulations of the system with a larger spatial domain and weight function (2.7) in Section 5.

We specify the rotating input $I(x-ct)$ as being always non-negative and periodic upon the spatial domain $x \in [-L, L]$. A class of functions that fits this restriction is

$$I(x-ct) = I_0 \cos^2\left(\frac{x-ct}{2}\right) \tag{2.8}$$

where I_0 is the strength of this input, which we use for our analysis of the system in Sections 3 and 4. In the simulations of Section 5, where we extend our study to larger networks, we use a Gaussian input stimulus

$$I(x-ct) = I_0 e^{-(x-ct)^2/\sigma_I^2} \qquad x-ct \in [-L, L] \tag{2.9}$$

where I_0 is input strength, σ_I the input spatial scale, and the domain width L for the simulations in which we use this input. For the bulk of the paper, we use stimulus strengths I_0 high enough so that substantial portions of the network operate close to saturation. This is in light of the fact that we are modeling high contrast visual inputs (see Fig. 1). Ben Yishai and colleagues examined the effects of weak inputs in a ring

so that $I = I_0$ when $t \square 2nT$

function (2.6), on the spatial domain $x \in [-\pi, \pi]$, and rotating input with finite speed, so

$$u_t = -u - \theta + \int_{-\pi}^{\pi} w_0 + w_2 \cos(x - x') \times H(u(x', t - \tau)) \, dx' + I_0 \cos^2\left(\frac{x - ct}{2}\right)$$

$$\theta_t = \epsilon(-\theta + \alpha u) \tag{3.7}$$

In order to check if the ON state exists for particular

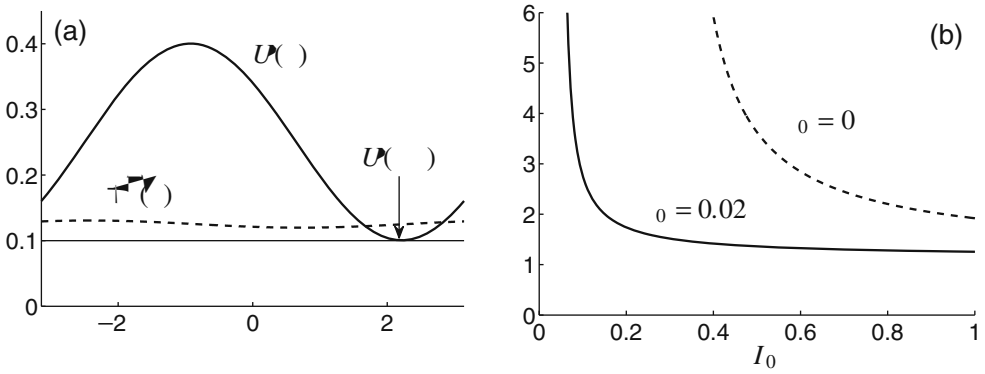
(a)
0.4
0.3
0.2
0.1
0
−2
0
2
(b)
6
5
4
3
2
1
0
0
0.2
0.4
0.6
0.8
1
I_0
$_0 = 0$
$_0 = 0.02$

$$V = \frac{I_0}{1+} + V_3 \sin + \cos - \frac{I_0}{2}\cos + I + V_4 \cos - \cos + \sin - \frac{I_0}{2}\sin + I \tag{3.17}$$

where

$$U_3 = \frac{c^2 + 1 +}{D}$$

$$U_4 = \frac{c^3 - + c}{D}$$

and

$$V_3 = \frac{c^2 - 1 +}{D}$$

$$V_4 = \frac{c + 1}{D}$$

Therefore, to specify the pulse width and associated shift to the input I, we impose self consistency by requiring that the input current U specified by Eq. (3.16) cross firing threshold at the leading and trailing edge of the pulse such that $U = U$

Fig. 6 Profiles of the
(**a**) stable and (**b**

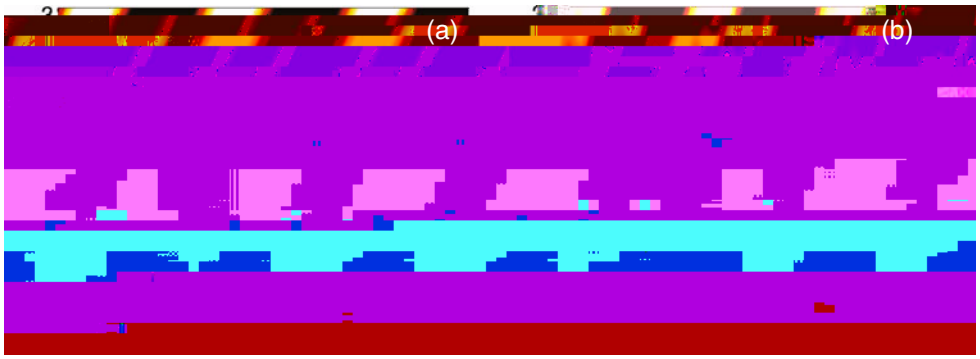

Fig. 8 Numerical simulations of stimulus-locked pulses and traveling breathers in the network with linear adaptation (2.1) for a Heaviside firing rate (2.5), where $u\ x\ t$ is plotted. (**a**) For a speed ($c = 0\ 2$) within the region of parameter space where stable locked traveling pulses exist. (**b**) For a speed ($c = 1$) beyond the critical speed where stable pulses cease to exist, superthreshold activity periodically lurches, representative of a discrete afterimage. Other parameters are $= 0\ 1$, $= 10$, $= 0\ 5$, $_0 = 0\ 02$, $_2 = 0\ 5$, and $I_0 = 0\ 5$

analysis proceeds by plugging these expressions in the system (2.1) along with the traveling pulse solutions (3.16) and (3.17). Upon expanding to first order in , we arrive at the linear equation

$$-c + + 1 + = \frac{-}{|U|} + \frac{- + -}{|U - |} - + + ^{-1} = \frac{}{} \tag{3.18}$$

where we have used the identity

$$\frac{\mathrm{d}H\ U\ -}{\mathrm{d}U} = \frac{-}{|U|} + \frac{- +}{|U - |} \tag{3.19}$$

In Folias and Bressloff (2005b), there is a detailed analysis of the complete spectrum of a similar linear operator on the infinite domain. We forgo such analysis here and focus particularly on the point spectrum of the operator in the system (3.18). In doing so, we can associate the point spectrum of the linear operator with the zeros of a complex analytic function called the Evans function (Coombes and Owen 2004). Thus, to predict the stability of stimulus-locked pulses, we look for nontrivial solutions of the eigenvalue problem (3.18). First, we note that the values which bound the essential spectrum $= -1 + ip$ and $= - ^{-1} + ip$ (p R) will not contribute to any instabilities. Omitting these values from the remainder of our analysis, we proceed by solving for the associated eigenfunctions. As we did in the solution of the existence problem, we can solve for in terms of to convert the system (3.18) to the following equation

$$\begin{aligned} -c + c + 1 + c\,1 + ^{-1} & - + ^{-1} + 1 + ^{-1} \\ &= \frac{}{|U|}\left[- - + ^{-1} - \right] \\ &\quad + \frac{-}{|U - |}\left[- + - + ^{-1} - + \right] \end{aligned}$$

By treating the pointwise terms and $-$ as constants, we can solve this equation as an inhomogeneous second order differential equation in the case of the harmonic weight function (2.6). Upon applying periodic boundary conditions, we arrive at the following expression for the eigenfunction

$$\begin{aligned} &= P_0 + \frac{P_1 \sin - P_2 \cos}{D_p}\ \frac{}{|U|} \\ &\quad + P_0 + \frac{P_1 \sin + - P_2 \cos +}{D_p} \\ &\quad \times \frac{-}{|U - |} \end{aligned} \tag{3.20}$$

where

$$P_0 = \frac{_0 + 1}{A_1}$$

$$P_1 = _2[\ ^2c^3 - cA_1 + c + 1\ A_2]$$

$$P_2 = _2[+ 1\ A_1 - c^2 + c^2A_2]$$

with

$$A_1 = \quad + 1 \quad + 1 \; +$$

$$A_2 = 2 \quad + \quad + 1$$

$$D_p = [\; c^2 - A_1]^2 + \; cA_2{}^2$$

Requiring self-consistency of the solution (3.20), we generate the following 2 × 2 linear system of equations

$= A_p$ where2

leaving a single unstable pulse whose linear stability is determined by a positive real eigenvalue. Nonetheless, the spatiotemporal dynamics of the network do evolve to a propagating pulse solution whose width changes periodically, as shown in Fig. 8.

3.4 Bumps

To consider the network dynamics resulting as the rotating input is slowed to a stop, we study the limit of the stimulus speed as $c \to 0$. In this case, there will be a stationary input, so we will look for stationary solutions,

Fig. 10(a), showing the wide bump is unstable and the thin bump is stable.

4 Nonlinear adaptation

Benda and Herz have derived a reduced firing rate model with an adaptation variable from three different conductance based models with hyperpolarizing currents thought to participate in spike frequency adaptation (Benda and Herz 2003). The adaptation variable has a nonlinear dependence upon the activity variable. Using this idea, a few studies have examined the effects that different forms of nonlinear adaptation have upon spatiotemporal dynamics of firing rate models (Coombes and Owen 2004, 2005; Kilpatrick and Bressloff 2010b). For example, Coombes and Owen (2005) showed that a neural field model with nonlinear adaptation can support breathing bumps and pulses as well as more exotic solutions without any spatially inhomogeneous input being applied (Folias and Bressloff 2004, 2005b). As has been shown in Kilpatrick and Bressloff (2010c), the stability analysis of bumps and traveling pulses in networks with nonlinear adaptation can be much more subtle than in the linear adapta-

Fig. 16 Profiles of the (**a**) stable for $c = 0\,2$ and (**b**) unstable pulse for $c = 0\,8$. Solutions U and V given by Eqs. (B.1) and (B.2), respectively. Note that the solution U remains above the threshold V $+_I$ within the region $\square$ $-$

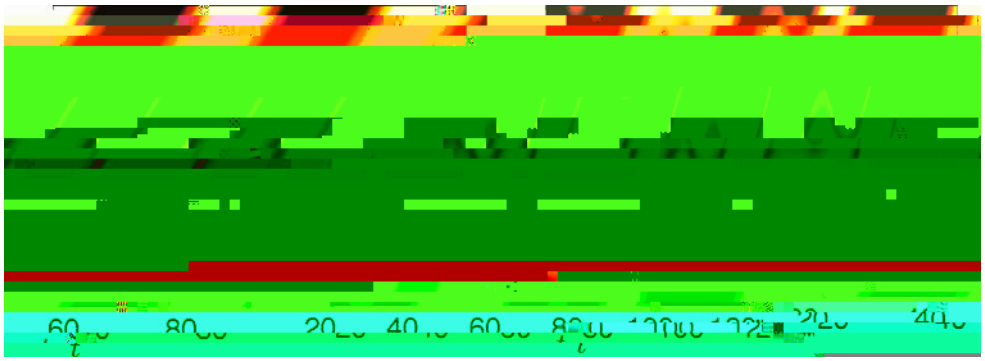

we find qualitatively similar results for the relationship between stimulus speed and the form of the resulting solution. In Fig. 20, we show two example simulations similar to that pictured in Fig. 8(b) for the Heaviside firing rate. The behavior of the model with a sigmoid firing rate, even for a fairly low gain of = 10, is quite similar to that with infinite gain. We found through numerical simulations that the switch from locked pulses to traveling breathers occurs at a stimulus speed of roughly $c = 0.4$, which is not too far removed from that predicted in the system with the Heaviside firing rate (2.5). Likewise, we found the onset of traveling breathers beyond a critical stimulus speed of roughly $c = 0.5$ for the network with a piecewise linear firing rate with slope = 2. For weak inputs (not shown), firing rate functions do not saturate but networks with continuous firing rate functions exhibit the same transitions between locked and breathing pulses and the speed at which the transition between these two behaviors decreases as synaptic modulation increases. When inputs become sufficiently weak, there is no transition to the ON state as c is increased to infinity, just as we found for networks with Heaviside firing rate.

We carried out such simulations for other parameter sets as well for both networks, with linear and nonlinear adaptation (not shown). Overall, it appears using a sigmoid with finite gain or a piecewise linear function does not drastically alter the dynamics existent in the system. Therefore we conclude that using the Heaviside firing rate for the bulk of our theoretical predictions in this paper is a reasonable approximation. In general, the firing rate of a neuron or population of neurons is known to be a continuous function input current. Therefore, the validity of our predictions in previous sections relies on the reduction of the firing rate to a piecewise constant function being a justifiable first order approximation.

Now, we turn to studying the networks with both a sigmoidal firing rate function (2.3) as well as the alternative weight function (2.7) in a larger periodic domain, specifically . In addition we use a Gaussian input stimulus (2.9) to the network. In general, we find similar results to those of the smaller network with for the transitions of stimulus-locked traveling

Research Fellowship (DMS-1004422). GBE is supported by an NSF grant (DMS-0817131).

Appendix A: ON state in system with nonlinear adaptation

In this appendix, we derive Eq. (4.3), giving the critical speed c at which the ON state ceases to exist in the full network with nonlinear adaptation (2.2). Thus, we study the equations,

$$u_t = -u +$$

$$+\frac{I_0}{2}+\frac{I_0[c\sin(\omega_I-\omega)-\cos(\omega_I-\omega)]}{2(1+c^2)}$$

$$+\frac{I_2[\sin(\omega)+c(1-\cos(\omega)]}{1+c^2}=\frac{1-e^{-(\omega)c}}{1-e^{-}}$$

terms as constants, to find

$$= \left(P_0 + \frac{P_1 \sin \quad - P_2 \cos}{D_p} \right) \left(- \right)$$

$$+ \left(- \right) \left(P_0 + P_1 \sin \quad + \right.$$

Bressloff, P. C., & Cowan, J. D. (2002). An amplitude equation approach to contextual effects in visual cortex. *Neural Computation, 14*(3), 493–525.

Bressloff, P. C., & Kilpatrick, Z. P. (2011). Two-dimensional bumps in piecewise smooth neural fields with synaptic depression. *SIAM Journal of Applied Mathematics, 71*(2), 379–408.

Chervin, R. D., Pierce, P. A., & Connors, B. W. (1988). Periodicity and directionality in the propagation of epileptiform discharges across neocortex. *Journal of Neurophysiology, 60*(5), 1695–1713.

Chossat, P., & Faugeras, O. (2009). Hyperbolic planforms in relation to visual edges and textures perception. *PLoS Computational Biology, 5*(12), e1000625.

Cohen, S., & Ditman, K. S. (1963). Prolonged adverse reactions to lysergic acid diethylamide. *Archives of General Psychiatry, 8*(5), 475–480.

Coombes, S. (2005). Waves, bumps, and patterns in neural field theories. *Biological Cybernetics, 93*(2), 91–108.

Coombes, S., & Owen, M. R. (2004). Evans functions for integral neural field equations with Heaviside firing rate function. *SIAM Journal on Applied Dynamical Systems, 3*(4), 574–600.

Coombes, S., & Owen, M. R. (2005). Bumps, breathers, and waves in a neural network with spike frequency adaptation. *Physics Review Letters, 94*(14), 148102.

Coombes, S., & Schmidt, H. (2010). Neural fields with sigmoidal firing rates: Approximate solutions. *Discrete and Continuous Dynamical Systems A, 28*(4), 1369–1379.

Dubois, J., & VanRullen, R. (2011). Visual trails: Do the doors of perception open periodically?

Shusterman, V., & Troy, W. C. (2008). From baseline to epileptiform activity: A path to synchronized rhythmicity in large–scale neural networks. *Physical Review E, 77*(6), 061911.

Stocker, M., Krause, M., & Pedarzani, P. (1999). An apamin-sensitive Ca2+-activated K+ current in hippocampal pyramidal neurons. *Proceedings of the National Academy of Sciences of the United States of America, 96*(8), 4662–4667.

Troy, W. C., & Shusterman, V. (2007). Patterns and features of